UNCERTAINTY IN THE SEISMIC RESPONSE OF REINFORCED CONCRETE STRUCTURES DUE TO MATERIAL VARIABILITY

C.L. Segura Jr.[1] and S. Sattar [2]

[1] *Research Structural Engineer, National Institute of Standards and Technology, Gaithersburg, MD USA,*
  christopher.segura@nist.gov
[2] *Research Structural Engineer, National Institute of Standards and Technology, Gaithersburg, MD USA, siamak.sattar@nist.gov*

Abstract

Inherent variability in the mechanical properties of reinforcing steel and concrete introduces uncertainty into the seismic assessment of reinforced concrete structures. Due to the high level of uncertainty associated with earthquake shaking characteristics, uncertainty due to variability in material properties is typically disregarded for seismic assessments. However, the potential impact of incorporating multiple sources of uncertainty in the seismic assessment framework is not well understood. To quantify the impact of material uncertainty, one-hundred iterations of a numerical model of a reinforced concrete structure are evaluated for their seismic performance at several earthquake shaking intensity levels. The one-hundred models differ only by the constitutive parameters used to model the materials, which are selected in accordance with measured statistical distributions of the mechanical properties of reinforcing steel bars and concrete. Material property statistical distributions, and correlations between material properties, are established using test data collected by the authors and test data available in the scientific literature. Preliminary results from analyses at the component level (i.e., individual column) indicate that dispersion in the predicted drift response for a given ground shaking intensity ($S_a[T_1]$) generally increases with shaking intensity, especially in the post-peak response regime for which a coefficient of variation (COV) in excess of 30 % is observed in the analyses presented herein. Of particular interest is the fact that a COV up to 20 % is observed for ground shaking intensities that produce only moderate ductility demands, prior to the onset of strength loss.

Keywords: uncertainty; performance-based earthquake engineering; seismic assessment; reinforced concrete

1. Introduction

Variability in the material properties of steel reinforcing bars and concrete affects the strength and deformation capacity of reinforced concrete structural components and, as a result, introduces uncertainty in the seismic assessment of reinforced concrete structures. Variability in material properties can be attributed to several factors including differences in the chemical composition of the steel and concrete materials, the source of the materials, and the material manufacturing processes. It is generally assumed that the contribution of material uncertainty to the overall uncertainty in the seismic assessment of a structure can be disregarded, particularly because of the relatively high level of uncertainty associated with earthquake shaking (record-to-record uncertainty). However, the potential impact of incorporating multiple sources of uncertainty, including that attributed to material variability, in the seismic assessment framework is not well understood. The importance of identifying and quantifying sources of uncertainty other than that associated with record-to-record variability has been highlighted by the results of recent blind prediction competitions in which relatively large dispersions have been reported for seismic response parameters predicted by experts in the field of nonlinear dynamic modeling of reinforced concrete structures [e.g., 1]. What is particularly concerning about the variability in contestant responses for blind prediction competitions is that the input earthquake shaking is known – that is, there is no record-to-record uncertainty.

The Performance-Based Earthquake Engineering (PBEE) framework [2,3] provides a convenient mechanism to account for the various sources of uncertainty that may impact the seismic assessment of structures. This paper describes the methodology used to quantify uncertainty due to variability in material properties. This work is one part of a project aimed at developing a framework to quantify the individual contributions of three main sources of uncertainty on the seismic response of reinforced concrete structures: 1) uncertainty associated with variability in material properties; 2) uncertainty related to the nonlinear modeling formulation used to conduct seismic analyses; and 3) uncertainty in earthquake shaking.

To evaluate the significance of material uncertainty, one-hundred iterations of a nonlinear structural analysis of a reinforced concrete structure are conducted at various earthquake shaking intensity levels. The one-hundred analysis iterations differ only by the constitutive parameters used to model the materials, which are selected in accordance with measured statistical distributions of the material properties of reinforcing steel and concrete, as well as correlations between material properties. To conduct the material uncertainty study, an analytical model representing a circular bridge column tested on the University of California, San Diego (UCSD) shake table in September 2010 [4] is developed. The UCSD bridge column structure is selected for uncertainty quantification because: 1) the bridge column is a simple structure that can be used to evaluate component-level uncertainty; 2) a blind prediction contest was organized and carried out by the UCSD research team [1] in coordination with the shake table test; and 3) comprehensive data are available on the experimental test.

The following sections describe: 1) the formulation of material statistical distributions used to conduct material uncertainty quantification; 2) the range of lateral drift predictions made by contestants of the UCSD blind prediction contest; 3) the development and verification of the analytical model of the bridge column; and 4) preliminary findings for the component-level (column) uncertainty study.

2. Statistical Variability in Material Properties

Variability in the mechanical properties of steel reinforcement and concrete is quantified as a set of statistical distributions and correlations developed using data available in the literature [5,6,7], an extensive database of steel reinforcing bar material tests provided to the authors courtesy of the Concrete Reinforcing Steel Institute (CRSI) [8], and a set of concrete cylinder tests collected by the authors. Material test data used by the authors consists of more than 80,000 tests on Grade 60 (f_y=420 MPa) reinforcing bars satisfying the requirements of ASTM A706 [9], as well as 88 concrete cylinder tests on normal-weight concrete with design compressive strengths between 31 MPa and 35 MPa. ASTM A706 places strict limits on the: 1) minimum and maximum

allowable yield strength, to control the forces that can develop in yielding members; 2) minimum allowable tensile strength; 3) minimum allowable tensile-to-yield strength ratio, to ensure adequate spread of plasticity at yielding sections; and 4) minimum allowable tensile rupture strain.

Statistical distributions are developed for material parameters that describe the monotonic stress-strain behavior of Grade 60 ASTM A706 reinforcement and concrete materials, idealized in Fig. 1a and Fig. 1b, respectively. Important material properties include the yield strength (f_y), elastic modulus (E_s), strain hardening modulus (E_{sh}), tensile strength (f_u), and rupture strain (ε_{rup}) of reinforcing steel, as well as the peak compressive stress-strain (ε_{c0}, f_{c0}) and crushing strain (ε_{cu}) of concrete (Fig. 1).
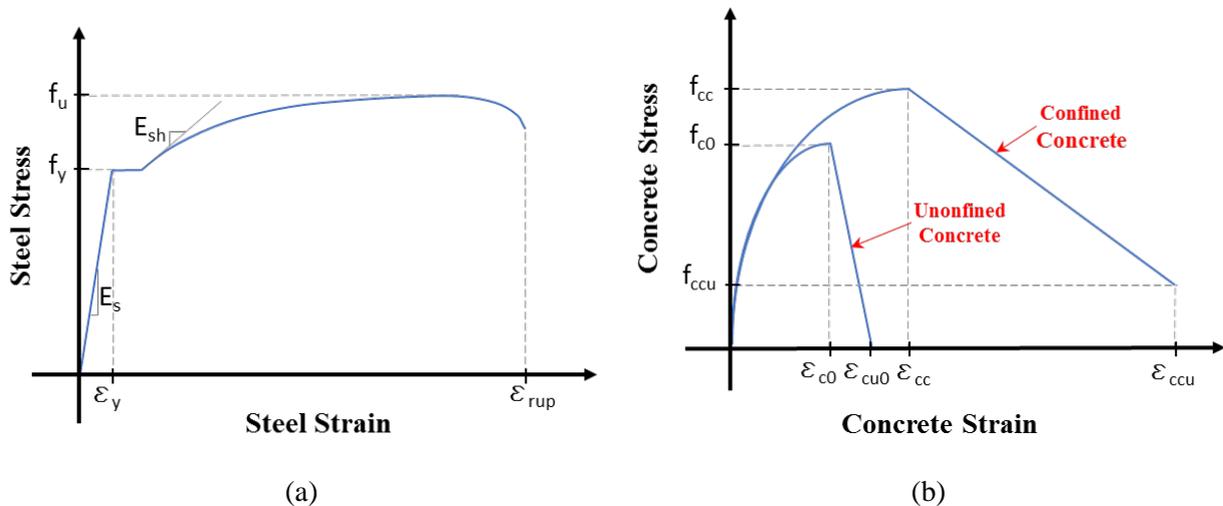
Fig. 1 – Theoretical Stress vs. Strain Behavior – (a) Reinforcing Steel in Tension; and (b) Concrete in Compression (Compressive Stress Shown as Positive)

For uncertainty quantification, material properties are represented as a set of statistical distributions. Fig. 2 provides a representative comparison of the experimental data to normal and lognormal probability distribution function (PDFs) (Fig. 2a) and cumulative distribution functions (CDFs) (Fig. 2b). Correlation coefficients between material properties are determined using a Spearman correlation analysis with a 95 % confidence criterion [10].

Confined concrete properties are not easily derived from test data because several factors contribute to the confined properties. However, confinement models that have been developed using laboratory tests that account for the various factors that affect the confined properties are available in the literature. Uncertainty in confined properties of concrete is quantified using the confinement models developed by Saatcioglu and Razvi [11] and Legeron and Paultre [12]. Specifically, statistical distributions for the peak confined stress-strain (ε_{cc}, f_{cc}) and confined concrete crushing strain (ε_{ccu}) are determined. Two additional confinement models [13,14] were evaluated, but both were deemed to introduce excessive dispersion in confined properties because the model was either developed specifically for rectangular sections, while the analyses reported herein are for a circular column, or because the method used to determine strains on the softening branch of the confined stress-strain curve is inconsistent with the other confinement models [15].

(a)   (b)
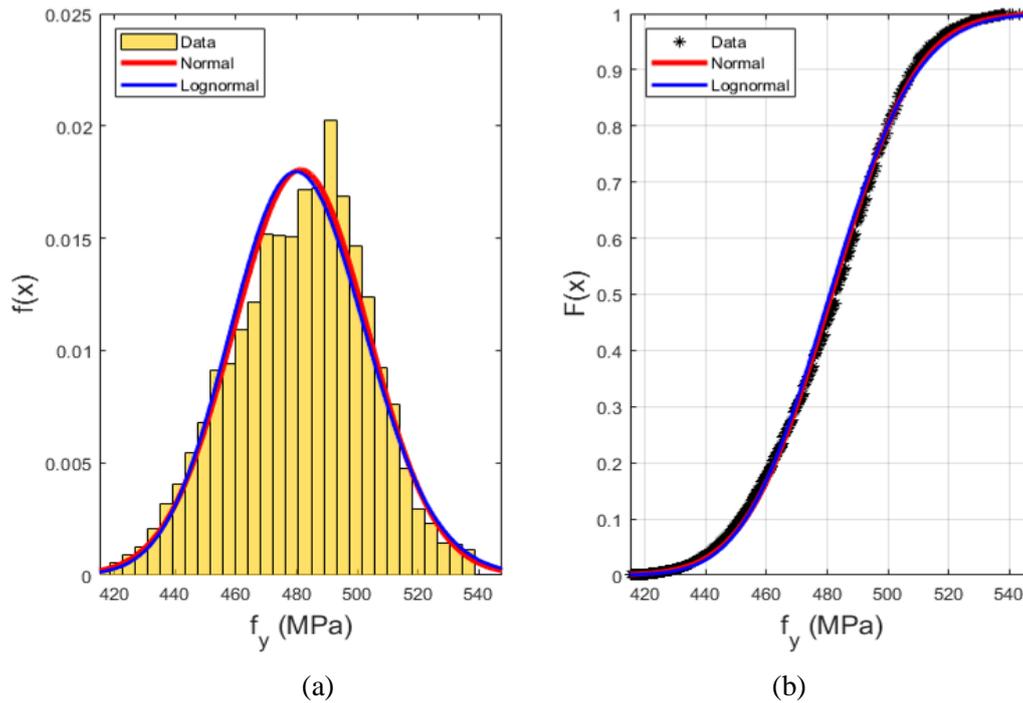
Fig. 2 – Measured Reinforcing Steel Yield Strength (f_y) – (a) Comparison of Histogram to PDF; and (b) Comparison of Measured Values to CDF

3. Model Development and Verification

3.1 UCSD Shake Table Test and Blind Prediction Contest

The impact of material uncertainty is quantified by evaluating the seismic performance of an analytical model representing a circular bridge column tested on the University of California, San Diego (UCSD) shake table in September 2010 [4]. A photo of the shake table test setup and a cross-sectional drawing of the column are provided in Fig. 3. The column was 1219 mm in diameter and 7315 mm in height. A large concrete mass with

(a)   (b)
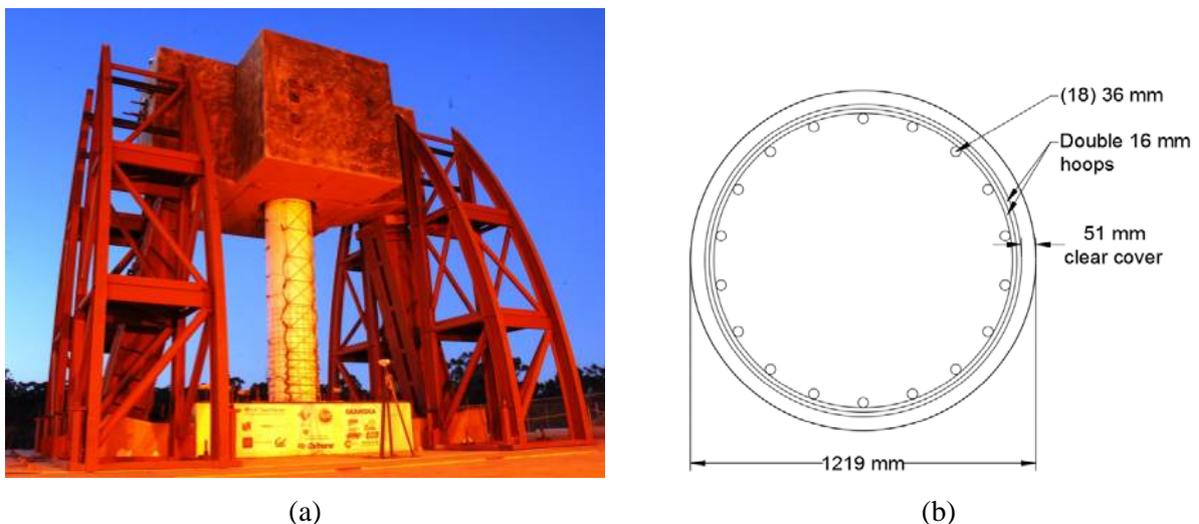
Fig. 3 – UCSD Bridge Column Shake Table Test – (a) Test Setup; and (b) Column Cross-Section [4]

a total tributary weight of 2.32 MN was attached to the top of the column (Fig. 3). Longitudinal reinforcement consisted of eighteen 36 mm diameter bars spaced evenly about the circumference of the column. Transverse reinforcement consisted of two bundled 16 mm diameter hoops spaced at 152 mm on-center. All reinforcement was specified as Grade 60 (f_y=414 MPa) ASTM A706 and the specified concrete compressive strength (f'_c) was 28 MPa. Measured concrete cylinder compressive strength at the time of testing was 41 MPa. Compressive strains at peak cylinder strength ranged between about 0.0025 and 0.003. The average yield strength and ultimate strength measured for two of the 36 mm diameter reinforcing bar samples were 518 MPa and 706 MPa, respectively, and average rupture strain for the rebar samples was 0.122 [4].

The bridge column was subjected to a series of six earthquake acceleration records, designated as EQ1 through EQ6, that were selected and scaled for target displacement ductility demands of 1.0 (EQ1), 2.0 (EQ2 and EQ4), 4.0 (EQ3 and EQ6), and 8.0 (EQ5). EQ2 and EQ4 used the same scaled record, as did EQ3 and EQ6 [1,4]. Fig. 4a compares maximum drift ratios predicted by the forty-two participants of the blind prediction contest to the experimentally measured responses for the six applied ground motion records. The mean of the predicted responses is also plotted in Fig. 4a. The relative difference in the mean predicted response and the experimentally measured drift ratio (i.e., mean bias) ranges between -6 % (EQ1) and -33 % (EQ6), indicating that the analytical models, on average, tend to underestimate the deformation of the bridge column. Fig. 4b presents boxplots of the contestant predictions for each earthquake record. For each boxplot, the bottom and top edges of the "box" indicate the extents of the data within one standard deviation of the mean of the predicted responses; the top and bottom "whiskers" indicate data within 2.7 standard deviations of the mean; and the "+" markers indicate outliers from a normal distribution. Relatively large dispersion in the predicted response is evident – particularly for EQ3, EQ5 and EQ6 – demonstrating the importance of quantifying potential sources of uncertainty in the seismic assessment framework.

(a)   (b)
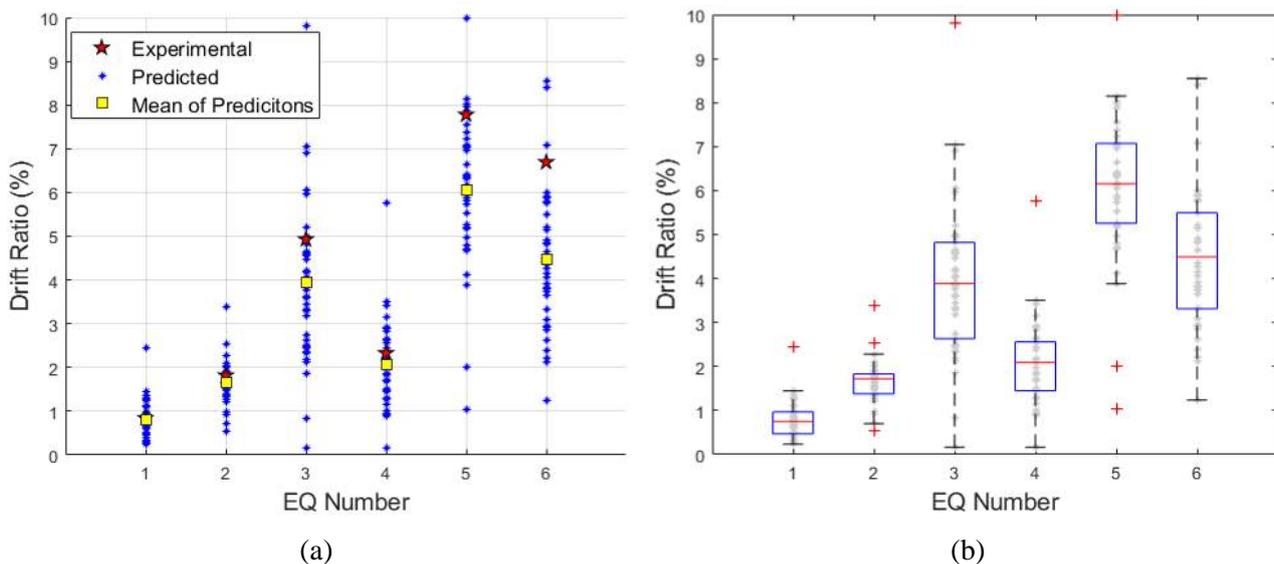
Fig. 4 – UCSD Blind Prediction Contest Responses – (a) Comparison of Predicted Drift Ratio to Experimental and Mean; and (b) Boxplot of Predicted Responses

3.2 Analytical Model Description

A distributed plasticity model (i.e., fiber model) of the bridge column is developed and nonlinear analyses are conducted in OpenSees [16]. A fiber element formulation is selected because, unlike lumped plasticity models, fiber models enable direct definition of material constitutive properties, thereby making it possible to straightforwardly quantify uncertainty due to variability in material properties. A displacement-based fiber

element model (stiffness formulation) is developed and verified against experimental measurements from the UCSD shake table test. The spatial discretization of the fiber model is shown in Fig. 5. The model consists of eight equal length elements, each with three Gauss-Lobatto integration points (Fig. 5a) [17]. An axial load of 2.32 MN is applied at the top node of the column model (Fig. 5a) and held constant throughout the analyses. A lumped mass of 237 000 kg (i.e., 2.32 MN/g_a) is also applied at the top node of the column. Confined concrete is discretized into 8 sections in the radial dimension of the column and 8 sections in the circular direction for a total of 64 confined concrete fibers (Fig. 5b). A total of 32 fibers (4 radial, 8 circular) are used to model unconfined cover concrete. Steel reinforcing bars are discretized into 18 fibers located at the centroid of the bar locations indicated in Fig. 3. Second-order P-Delta effects are accounted for in the nonlinear analyses.

The Concrete02 constitutive model implemented in OpenSees is used to model unconfined concrete. Confined concrete is modeled using the Concrete07 constitutive model and steel reinforcing bar materials are modeled using the SteelMPF model, both of which employ sophisticated constitutive hysteretic rules [18,19,20]. Regularization of the compressive material properties for concrete and steel is conducted in accordance with the technique developed by Coleman and Spacone [21]. The regularization technique adjusts the stress-strain relationships for uniaxial fibers such that analytical results are insensitive to the model spatial discretization. The OpenSees MinMax constitutive model is used to assign tension and compression strain limits for the SteelMPF reinforcing bar constitutive model. The tension strain limit is set as the steel rupture strain capacity while the compression strain limit signals the reinforcing bar material to degrade to zero stress (i.e., rebar buckling) once the confined concrete reaches its crushing strain.
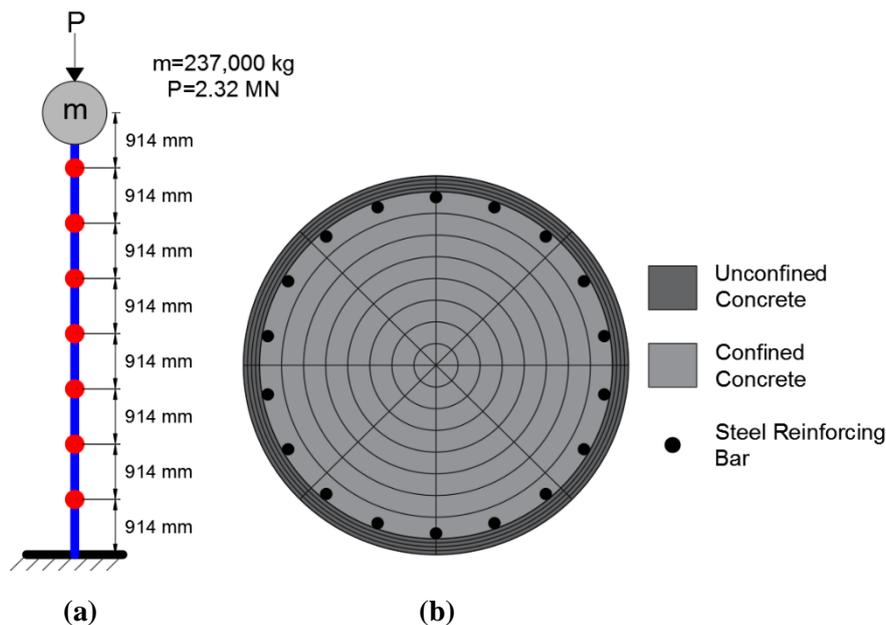

Fig. 5 – Analytical Model Discretization – (a) Elements and Nodes; and (b) Cross-Section

3.3 Model Verification

Model verification is conducted by comparing the response of the analytical model to the response measured experimentally on the shake table at UCSD. To do so, the analytical model is subjected to the acceleration time series applied during the UCSD shake table test, which consisted of six earthquake acceleration records applied separately. A comparison of the analytical and experimentally measured lateral drift ratio, measured at the top of the column, is shown in Fig. 6. Only the experimental deformation attributed to flexure is plotted in Fig. 6 to enable a direct comparison with the results for the fiber element model, which is only capable of capturing

the flexural response of the column. It is evident in Fig. 6 that the analytical model is capable of capturing the deformation response of the bridge column, including residual inelastic deformations. For each earthquake record, the maximum analytical and experimental drift ratio are compared in Fig. 6. The difference in the predicted and experimental maximum drift ratio ranges between 3 % (EQ3) and 29 % (EQ5). It is emphasized that model parameters are not "calibrated" to achieve the results presented in Fig. 6; rather, the uniaxial fiber material parameters are taken directly from the measured material properties [4] and confinement models, adjusted for mesh size in accordance with the material regularization technique developed by Coleman and Spacone [21].
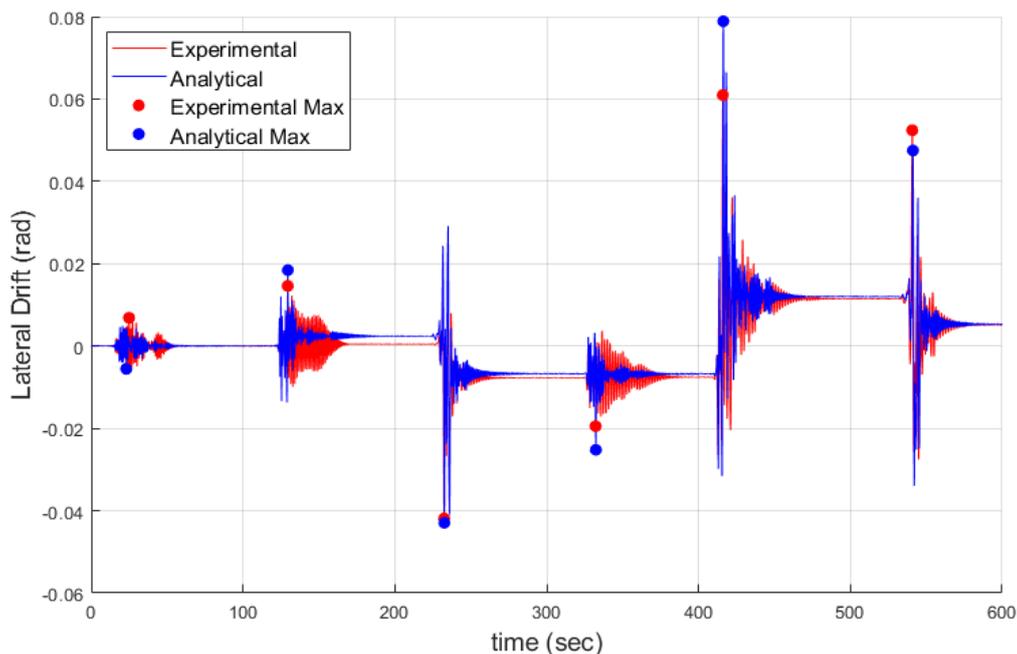
**Fig. 6 – Model Verification – Experimental vs. Analytical Lateral Drift Ratio**

4. Uncertainty Quantification

One-hundred iterations of the analytical model (Fig. 5) are constructed and nonlinear analyses are conducted in OpenSees to quantify the impact of uncertainty in the material properties of reinforcing steel and concrete. The one-hundred iterations of the analytical model are the same in their formulation (Fig. 5), differing only by the material properties used to define the constitutive behavior of the fiber elements. The input constitutive parameters for each model are selected from a set of one-hundred realizations of reinforcing steel, unconfined concrete, and confined concrete material properties. Mean, minimum, and maximum values of the one-hundred material realization set are given in Table 1 for three representative material properties (f_{c0}, f_y, and ε_{rup}). The one-hundred material property realizations are selected to represent the statistical distributions of the material properties, and correlations between properties, described in Section 2 with minimal variation from the desired statistical distributions. The variation in the mean and coefficient of variation for the one-hundred material realization set and the statistical distributions is below 5 % for all material properties.

Table 1: Ranges of Representative Material Properties (See Fig. 1 for Description of Properties)

	Mean	Minimum	Maximum
f_{c0}	33.8 MPa	23.5 MPa	46.4 MPa
f_y	482 MPa	429MPa	529 MPa
ε_{rup}	0.157	0.107	0.211

Nonlinear analyses of the analytical models are conducted in OpenSees using an Endurance Time Acceleration Function (ETAF) (e.g., see [22]). ETAF enables the evaluation of the analytical model at progressively increasing ground shaking intensities using a single, unique ground acceleration record. ETAF is, therefore, analogous to a dynamic pushover analysis. A plot of ground acceleration vs. time for the ETAF is provided in Fig. 7a. Fig. 7b presents the 2.5 %-damped pseudo acceleration response spectra (S_a) for ten different target time intervals. A target time interval represents the elapsed time from the beginning of the record. For example, a target time of 10 seconds captures ground shaking for the time between 0 and 10 seconds, whereas a target time of 12 seconds captures ground shaking from time 0 to 12 seconds. As shown in Fig. 7b, the spectral acceleration demands for the ETAF record increase with increasing target time.

(a)   (b)
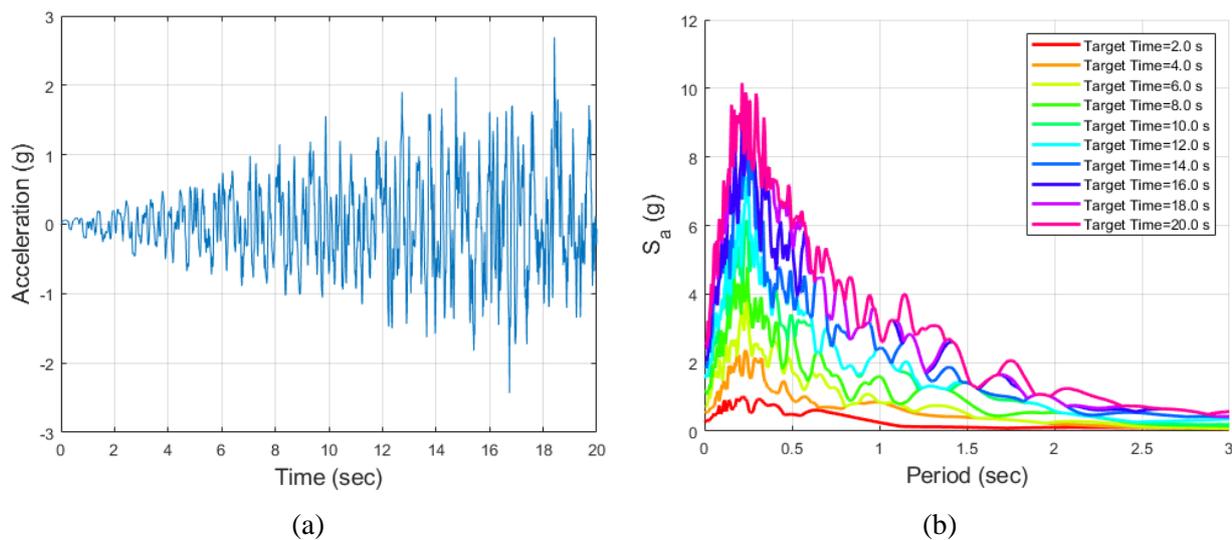
Fig. 7 – (a) Acceleration Record for ETAF; and (b) 2.5 %-Damped Response Spectra (S_a) at Various Target Times

Fig. 8a presents the lateral force vs. drift ratio backbone curves for ten representative analyses of the one-hundred model iterations. The models demonstrate very ductile response, as would be expected for the well-confined section with relatively low axial stress. For each model, the ultimate drift ratio from the analysis is indicated as a red circle on the figure. The ultimate drift ratio is designated as the lateral drift at the last analysis step for which the residual strength exceeds 80 % of the peak capacity (i.e., 20 % strength loss). Variability in the column shear force is evident beyond a drift ratio of about 1 %; however, as shown in Fig. 8b, dispersion in the deformation response of the column is small until the onset of strength loss. Following strength loss, a wide range of deformation responses is evident. The coefficient of variation of the predicted lateral drift ratio ranges between 2.5 % and 8 % for lower earthquake shaking intensities – that is, for target times less than about 8 seconds. For higher earthquake shaking intensities, following strength loss, coefficients of variations reach approximately 16 %.
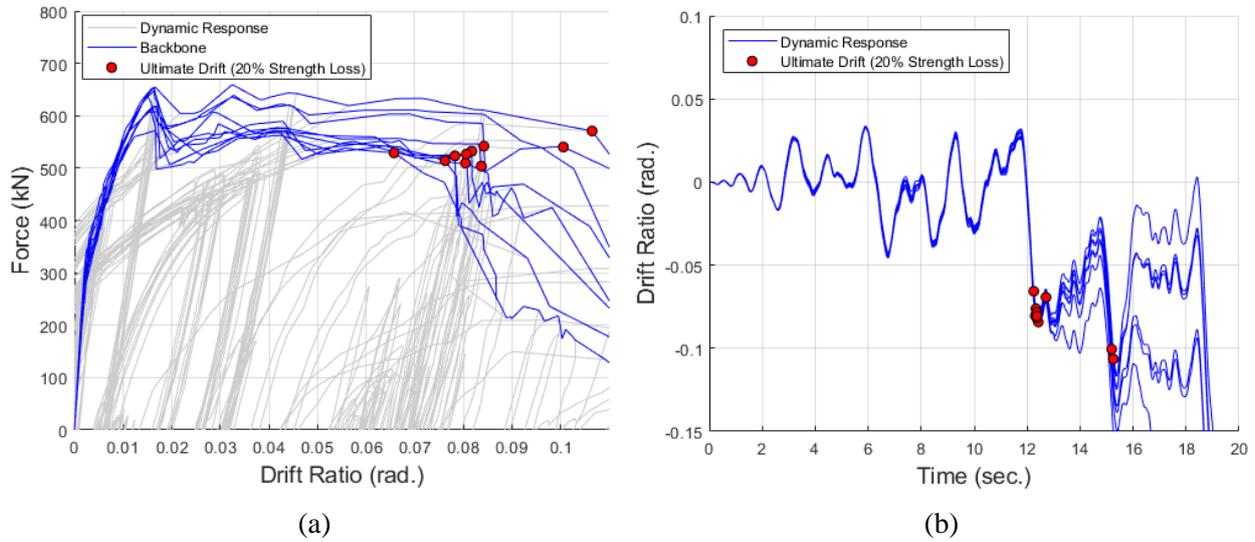
Fig. 8 – (a) Lateral Force vs. Drift Ratio; and (b) Drift Ratio Time Series

Overall, dispersion in the predicted deformation response of the column for a particular analysis target time is within what is typically considered an acceptable range for seismic analysis [e.g., see 23,24]. It is important to point out, however, that in the PBEE framework [2,3], the vulnerability of a structure to collapse is often expressed in terms of the probability of reaching a particular engineering demand parameter (EDP) at a given ground shaking intensity. The EDP and the ground shaking intensity measure often used to characterize collapse risk are the maximum lateral drift (Δ_{max}) and the first mode elastic spectral acceleration ($S_a[T_1]$), respectively. Characterization of the dispersion in Δ_{max} for a given $S_a(T_1)$ is, therefore, important to account for uncertainty in the PBEE framework. To illustrate this dispersion, the predicted Δ_{max} values determined for the one-hundred model iterations are presented as lognormal PDFs in Fig. 9 for three earthquake shaking intensity levels: $S_a(T_1)=0.5g$, $S_a(T_1)=1.5g$, and $S_a(T_1)=3.0g$. The best-fit distribution based on the Kolmogorov–Smirnov test at different shaking intensities may differ. A lognormal distribution is used herein because it is commonly used in the field of structural engineering to represent the uncertainty in the lateral drift response of structures. A modal damping coefficient of 2.5 % is assumed for the spectral accelerations in Fig. 9, as is the case for the spectra shown in Fig. 7b. As can be seen in Fig. 9, dispersion generally increases for increasing $S_a(T_1)$. For smaller spectral acceleration demands (i.e., $S_a[T_1]=0.5g$), the dispersion in drift ratio is low. This is expected as the column response is primarily elastic for this level of shaking. As yielding of the column's longitudinal reinforcement occurs (i.e., $S_a[T_1]=1.5g$), dispersion in Δ_{max} increases. Strength loss is observed in most of the one-hundred models for $S_a[T_1]>2g$, after which dispersion in the predicted drift response becomes large in proportion to the variability in $S_a(T_1)$. A similar trend of increasing dispersion in the lateral drift response for higher earthquake shaking intensity levels has been observed for steel columns [25]. It is noted that, due to the use of the ETAF loading protocol (Fig. 7), drift ratio results for larger $S_a(T_1)$ values include previous damage associated with lower $S_a(T_1)$ values.

Table 2 summarizes statistical parameters for the lognormally distributed Δ_{max} at the three ground shaking intensities shown in Fig. 9. The mean ($\overline{\mu}_{\Delta_{max}}$) and median ($\tilde{\mu}_{\Delta_{max}}$) values reported in Table 2 are calculated according to Eqns. 1 and 2, respectively:

$$\overline{\mu}_{\Delta_{max}} = e^{\mu_{\ln(x)}+\frac{1}{2}\sigma_{\ln(x)}^2}, \tag{1}$$

$$\tilde{\mu}_{\Delta_{max}} = e^{\mu_{\ln(x)}}, \tag{2}$$
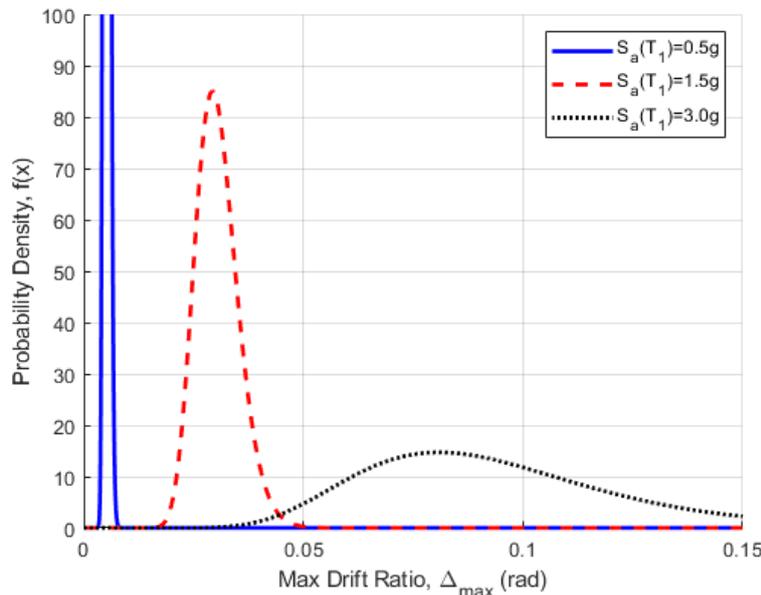
Fig. 9 – PDF of Maximum Drift Ratio for Different $S_a(T_1)$

where $\mu_{\ln(x)}$ and $\sigma_{\ln(x)}$ are the mean and standard deviation of the natural logarithms of drift values. The coefficient of variation reported in Table 2 is calculated according to Eqn. 3:

$$COV_{\Delta_{\max}} = \sqrt{e^{\sigma_{\ln(x)}^2} - 1}. \tag{3}$$

For ground shaking intensities that result in elastic response of the column model (e.g., $S_a[T_1]$=0.5g), the coefficient of variation for $\Delta_{\max}$ is generally around 10 % or less. In the inelastic response regime, prior to the onset of strength loss (e.g., $S_a[T_1]$=1.5g), the dispersion in $\Delta_{\max}$ becomes larger, reaching a coefficient of variation up to approximately 20 %. The largest dispersion in the predicted drift response (e.g., COV≈30 % for $S_a[T_1]$=3.0g) is associated with a reduction in the lateral load-carrying capacity of the column (softening). The larger dispersion in the softening regime is attributed to the uncertainty in the post-peak behavior of the confined concrete material.

Table 2: Statistical Parameters of $\Delta_{\max}$ for Different $S_a(T_1)$

$S_a(T_1)$	Mean ($\bar{\mu}_{\Delta_{\max}}$)	Median ($\tilde{\mu}_{\Delta_{\max}}$)	Coefficient of Variation ($COV_{\Delta_{\max}}$)
0.5g	0.53 %	0.52 %	10.8 %
1.5g	3.04 %	3.01 %	15.9 %
3.0g	9.42 %	8.95 %	32.7 %

5. Summary

A methodology to quantify uncertainty in the seismic assessment of structures due to variability in the mechanical properties of concrete and reinforcing steel is presented. This material uncertainty quantification study is one part of an ongoing project aimed at developing a framework to quantify the individual

contributions of uncertainty on the seismic response of reinforced concrete structures, at both the component level (individual column) and at the system level (frame) due to: (1) variability in material properties, (2) the choice of nonlinear modeling formulation used to conduct seismic analyses, (3) and earthquake shaking. Uncertainty in the seismic response of a structural component is quantified using one-hundred iterations of an analytical model of a reinforced bridge concrete column. The one-hundred model iterations capture the statistical distributions of concrete and reinforcing steel mechanical properties determined using data collected by the authors and data available in the scientific literature. Analytical seismic responses at various earthquake shaking intensities (i.e., $S_a[T_1]$) are determined for the one-hundred models using an Endurance Time Acceleration Function, which subjects the model to increasing seismic demands using a single ground acceleration record. Results of the component level study demonstrate that dispersion in the predicted drift response due to material variability generally increases with increasing $S_a(T_1)$. In the elastic response regime, dispersion is low (coefficient of variation, COV, around 10 % or less); however, as flexural yielding occurs, dispersion increases (COV up to 20 %) even though a hardening response is still evident in the models. Larger dispersion in the post-peak regime (COV around 30 %) can be attributed to greater uncertainties in the material response of concrete as material softening occurs.

6. Acknowledgements

7. References

[1] Terzic, V., Schoettler, M.J., Restrepo, J.I., and Mahin, S.A. (2015): Concrete Column Blind Prediction Contest 2010: Outcomes and Observations. *Technical Report PEER 2015/01*, Pacific Earthquake Engineering Research, Berkeley, USA.

[2] Porter, K.A. (2003): An Overview of PEER's Performance-Based Earthquake Engineering Methodology. *Ninth International Conference on Applications of Statistics and Probability in Civil Engineering (ICASP9)*, San Francisco, USA.

[3] Moehle, J. and Deierlein, G.G. (2004): A Framework Methodology for Performance-Based Earthquake Engineering. *13th World Conference on Earthquake Engineering*, Vancouver, Canada.

[4] Schoettler, M.J., Restrepo, J.I., Guerrini, G., Duck, D.E., and Carrea, F. (2015): A Full-Scale, Single-Column Bridge Bent Tested by Shake Table Excitation. *Technical Report PEER 2015/02*, Pacific Earthquake Engineering Research, Berkeley, USA.

[5] Mirza, S.A. and MacGregor, J.G. (1979): Variability of Mechanical Properties of Reinforcing Bars. *ASCE Journal of the Structural Division*, **105** (5), 921-937.

[6] Mirza, S.A., Hatzinikolas, M., and MacGregor, J.G. (1979): Statistical Description of Strength of Concrete. *ASCE Journal of the Structural Division*, **105** (6), 1021-1037.

[7] Nowak, A.S., Szersen, M.M., Szeliga, E.K., Szwed, A., and Podhorecki, P.J. (2008): Reliability-Based Calibration for Structural Concrete, Phase 3. *Report to the Portland Cement Association and Precast/Prestressed Concrete Institute*, Skokie, USA.

[8] CRSI (2018): CRSI Mill Database. *Annual Summary Reports for 2011-2017*. Concrete Reinforcing Steel Institute (CRSI), Schaumburg, USA.

[9] ASTM A706/A706M (2016): Standard Specification for Deformed and Plain Low-Alloy Steel Bars for Concrete Reinforcement. American Society for Testing and Materials (ASTM) International, West Conshohocken, USA.

[10] Spearman, C. (1904): The Proof and Measurement of Association Between Two Things. *The American Journal of Psychology*, **15** (1), 72-101.

[11] Saatcioglu, M. and Razvi, S.R. (1992): Strength and Ductility of Confined Concrete. *ASCE Journal of Structural Engineering*, **118** (6), 1590-1607.

[12] Legeron, F. and Paultre, R. (2003): Uniaxial Confinement Model for Normal- and High-Strength Concrete Columns. *ASCE Journal of Structural Engineering*, **129** (2), 241-252.

[13] Mander, J.B., Priestley, M.J.N., and Park, R. (1988): Theoretical Stress-Strain Model for Confined Concrete. *ASCE Journal of Structural Engineering*, **114** (8), 1804-1826.

[14] Scott, B.D., Park, R., and Priestley, M.J.N. (1982): Stress-Strain Behavior of Concrete Confined by Overlapping Hoops at Low and High Strain Rates. *ACI Journal*, **79** (1), 13-27.

[15] Arteta, C. A. (2015): Seismic Response Assessment of Thin Boundary Elements of Special Concrete Shear Walls. *PhD Dissertation*, University of California, Berkeley, USA.

[16] Mazzoni, S., McKenna, F., and Fenves, G.L. (2006): OpenSees Command Language Manual, University of California, Berkeley, Berkeley, USA.

[17] Abramowitz, M. and Stegun, I.A. (1964): Handbook of Mathematical Functions With Formulas, Graphs, and Mathematical Tables. *National Bureau of Standards Applied Mathematics Series*, National Bureau of Standards, Washington D.C., USA.

[18] Chang, G.A. and Mander, J.B. (1994): Seismic Energy Based Fatigue Damage Analysis of Bridge Columns: Part 1 – Evaluation of Seismic Capacity. *Technical Report for the National Center for Earthquake Engineering Research*. The University at Buffalo, State University of New York, Buffalo, USA.

[19] Menegotto, M., and Pinto, P.E. (1973): Method of Analysis of Cyclically Loaded RC Plane Frames Including Changes in Geometry and Non-Elastic Behavior of Elements Under Normal Force and Bending. *Symposium on Resistance and Ultimate Deformability of Structures Acted on by Well-Defined Repeated Loads*. Lisbon, Portugal.

[20] Filippou F.C., Popov, E.P., and Bertero, V.V. (1983): Effects of Bond Deterioration on Hysteretic Behavior of Reinforced Concrete Joints. *Report No. UCB/EERC-83/19*. Earthquake Engineering Research Center, University of California, Berkeley, Berkeley, USA.

[21] Coleman, J. and Spacone, E. (2001): Localization Issues in Force-Based Frame Elements. *ASCE Journal of Structural Engineering*, **127** (11), 1257-1265.

[22] Hariri-Ardebili, M.A., Sattar, S., and H. E. Estekanchi (2014): Performance-based Seismic Assessment of Steel Frames Using Endurance Time Analysis. *Engineering Structures*, **69**, 216-234.

[23] FEMA (2009): Quantification of Building Seismic Performance Factors (FEMA P695). *FEMA P695*, Prepared by the Applied Technology Council for the Federal Emergency Management Agency (FEMA), FEMA, Washington D.C., USA.

[24] FEMA (2000): Recommended Seismic Design Criteria for New Steel Moment-Frame Buildings (FEMA 350). *FEMA 350*, Prepared by the SAC Joint Venture for the Federal Emergency Management Agency (FEMA), FEMA, Washington D.C., USA.

[25] Sattar, S., Weigand, J.M, and Wong, K.K.F. (2018): Quantification of Uncertainties in the Response of Beam-Columns in Steel Moment Frames. *11th U.S. National Conference on Earthquake Engineering*, Los Angeles, USA.